Thin Solid Films 562 (2014) 554–560

Contents lists available at ScienceDirect

Thin Solid Films

journal homepage: www.elsevier.com/locate/tsf

Three ranges of the angular dependence of critical current of $BaZrO_3$ doped $YBa_2Cu_3O_{7-\delta}$ thin films grown at different temperatures

M. Malmivirta [a,*], L.D. Yao [b], H. Huhtinen [a], H. Palonen [a,c], S. van Dijken [b], P. Paturi [a]

[a] Wihuri Physical Laboratory, Department of Physics and Astronomy, University of Turku, FI-20014 Turku, Finland
[b] NanoSpin, Department of Applied Physics, Aalto University, School of Science, P.O. Box 15100, FI-00076 Aalto, Finland
[c] The National Doctoral Programme in Nanoscience (NGS-NANO), Turku, Finland

ARTICLE INFO

Article history:
Received 10 October 2013
Received in revised form 28 April 2014
Accepted 30 April 2014
Available online 14 May 2014

Keywords:
High-temperature superconductor
Yttrium barium copper oxide
Barium zirconate
Thin films
Transmission electron microscopy
Flux pinning
Columnar defects

ABSTRACT

The growth of $BaZrO_3$ (BZO) in pulsed laser deposited $YBa_2Cu_3O_{7-\delta}$ (YBCO) thin films was studied by varying the deposition temperature. It was found that there are three deposition temperature ranges based on the properties of $J_c(\theta)$, the angular dependence of critical current density. Samples made at a relatively low temperature (low-T samples) do not show a *c*-axis peak in $J_c(\theta)$ whereas mid-T samples exhibit a peak as *B* *c*-axis of YBCO. In high-T samples the *c*-peak disappears again. In the low-T samples BZO rods are too splayed and short for a *c*-axis peak whereas in the high-T samples vortices move along correlated, but shortened rods as well as along stacking faults, which causes the *c*-axis peak to disappear. The superconducting properties of the films were studied with both magnetic and transport measurements and the structural properties were characterized using X-ray diffraction and transmission electron microscopy. Correlations between the structural and superconducting properties were analyzed using the vortex path model.

1. Introduction

The properties of $YBa_2Cu_3O_{7-\delta}$ (YBCO) thin films have been improved in the past years by many methods [1]. The most used way is to dope YBCO with a non-superconducting second phase, *e.g.* $BaZrO_3$ (BZO) [2–4], which forms either nanodots or nanorods in the YBCO matrix. In addition to increasing the critical current absolute values, BZO nanorods also affect the angular dependence of critical current, $J_c(\theta)$, where usually a broad peak is seen [4] when *B* *c*-axis of YBCO. It has been noted that while the density of rods changes with different doping concentrations, the radius of the rods stays about the same [5]. Also, it has been estimated that the rods that form do not consist entirely of BZO, but about half of rod volume contains distorted YBCO [6] and the rod is surrounded by distorted YBCO with dislocations [7]. On the other hand, in a study by Maiorov et al. [8] it was found that the rods consist merely of BZO in BZO and Y_2O_3 co-doped YBCO. The lattice mismatch between YBCO and BZO is about 9% which explains the strain and distortion of the YBCO–BZO-lattice. The strain also gives a plausible explanation for the columnar growth of BZO [9]. In a similar way, the growth of InAs columns on GaAs(100)-surface has been attributed to differences in lattice parameters [10].

The effect of deposition temperature on pulsed laser deposited (PLD) YBCO films has been studied before. In undoped YBCO, the stacking fault densities increase with deposition temperature [11], which enhances the critical current densities in a magnetic field. Also, other defect-related effects and possibly a Ba–Cu–O liquid phase during growth has been attributed to growth temperature [12]. In the latter case, an abrupt change of the shape of $J_c(\theta)$ and a drop of J_c near *ab*-peak were seen with increasing deposition temperature. The effects in BZO doped films provide similar kind of pinning improvements. The lengthening of the plateau region in $J_c(B)$-curves and the shift of the flux pinning force density maximum to higher fields with elevated deposition temperature have been attributed to correlated pinning centers [13,14]. Within the deposition temperature window used in Refs. [8] and [9] the length of the rod has been seen to increase and splay has been found to decrease with increasing deposition temperature both for BZO and BZO and Y_2O_3 co-doped YBCO. The deposition temperature does not only affect the structure but also the growth mode of pure YBCO; low substrate temperatures produce spiral growth while at higher temperatures (normal conditions) 2D nucleation and growth is favored during pulsed laser deposition [15].

In this paper, we study the effect of growth temperature in BZO doped PLD YBCO thin films. The film structures were characterized with X-ray diffraction and transmission electron microscopy (TEM). The superconducting properties were determined using

* Corresponding author.
E-mail address: mika.malmivirta@utu.fi (M. Malmivirta).

http://dx.doi.org/10.1016/j.tsf.2014.04.093
0040-6090/

magnetic measurements and also the angular dependencies of critical currents were measured. The results are interpreted with the vortex path model for angular dependencies of critical currents. The structural results are connected to the superconducting properties.

2. Experimental details

The films were grown with a pulsed laser deposition (PLD) system on 5×5 mm^2 $SrTiO_3$ (100) substrates using a 5 wt.% BZO doped nanostructured YBCO target (prepared as described in [16]). The deposition system is described in more detail in [17]. The deposition temperature T_{dep} was varied between 700 and 850 °C in 25 °C steps and after ablation each film was oxygenated at 50 °C below T_{dep} in an atmospheric pressure of O_2 for 10 min. Ablation was done with a XeCl excimer laser ($\lambda = 308$ nm) in an oxygen pressure of 23 Pa. Based on the properties of the $J_c(\theta)$ curves of the films, they were grouped into three categories: low-, mid- and high-T groups where T refers to deposition temperature. The boundary between low- and mid-T categories is about 700–725 °C and between mid- and high-T is about 800–825 °C. In each category, several films were made with different deposition temperatures. Because there are no major differences between the films in the same category, the properties of mainly one film is presented from each group.

The crystal structures were examined with an X-ray diffractometer (Philips X'pert Pro with Schulz texture goniometer). To check the purity of the films, θ–2θ scans with $\psi = 0$ were measured between 20° and 70°. Also, more accurate θ–2θ and rocking curve scans were performed on the YBCO (005) peak. To determine the growth of BZO, similar θ–2θ and rocking curve scans were made for BZO (002). The crystal growth direction was determined by 2θ–ϕ scans for YBCO (102) with two different ψ for *c*- and *a*-axis oriented grains. Similar 2θ–ϕ scans were taken of YBCO (212) to quantify twinning [18]. In addition to this, a 2θ–ϕ scan for BZO (110) was made. The microstructure of the films was analyzed by electron transmission microscopy using a JEOL 2200FS TEM instrument with double Cs correctors, operated at 200 keV. All cross-sectional TEM specimens were prepared by a modified mechanical polishing method; a Si/film/Si sandwich structure was firstly glued by epoxy after which it was cut into thin slices. After that, the thin slices were ground and polished by a MultiPrep polishing system (Allied High Tech products, Inc.), and finally milled in an Ar ion polishing system (Model 691 PIPS, Gatan Inc.).

The magnetic and superconducting properties were determined with a Quantum Design Physical Property Measurement System (PPMS). The onset critical temperature T_c was defined with the ACMS option of the PPMS from the onset temperature of the in-phase component of the AC-magnetization. DC-magnetization was measured between −8 and 8 T at 10 and 77 K and from these measurements the critical current was calculated using the Bean formula [19]. The angular dependencies of the critical currents were measured using the horizontal rotator option in magnetic fields between 0.5 and 8 T and at angles between 0° and 360° in the maximum Lorentz force configuration using 3° steps. For these measurements, each sample was patterned with wet chemical etching. The etched pattern was a standard four probe measurement circuit with a 50 μm wide current stripe. The contacts on the samples were made by tapping with indium. Measurements were done at temperatures 10–70 K in 10 K steps for all fields and angles. The values for voltage between the voltage pads as a function of applied current were recorded with the critical electric field of 215 μV/cm. On some samples the critical value was increased slightly to deal with the noise. However, the shape of the $J_c(\theta)$-curve did not change with the voltage limit [20].

3. Results and discussion

3.1. Structural properties

By scanning the YBCO (102) peak in *a*- and *c*-axis configurations, it was assured that there were no *a*-axis oriented grains in any of the samples. In scans of the YBCO (212) peak set, peak splits due to twinning are clearly seen for high-T samples and slightly less clearly in the other group, but the width of the four peak set stays approximately constant in 2θ- and ϕ-directions throughout different deposition temperatures. The splits in high-T films indicate that the structure of high-T samples is slightly more relaxed than that of the low- and mid-T samples. Rocking curves of YBCO (005) showed full width at half maximum (FWHM) values of 0.2°–0.3° with no clear dependence on deposition temperature. The values are similar to what has been found before [21,14]. According to these results, the YBCO matrix does not contain out-of-plane oriented grains. Also the oxygen content of YBCO lattice was estimated by comparing the intensities of (00*l*) YBCO peaks in θ–2θ-diffractograms. $I(005)/I(004) < 20$ and $I(005)/I(007)$ is between 7 and 10, and thus $\delta < 0.1$ [22] for all films.

BZO, on the other hand, shows a stronger dependence on T_{dep}. The evolution of its (002)-peak as a function of T_{dep} (Fig. 1) clearly shows a change of the BZO lattice parameters with T_{dep}. At low temperatures the peak is seen at a higher 2θ angle than the corresponding peak of a bulk sample (vertical line in figure is calculated from data in [23]). At higher temperatures another peak forms at lower 2θ angle, close to the bulk value. In other words, with increasing deposition temperature the *c*-axis parameter rises from smaller than bulk to about the same as bulk. A similar evolution is found for BZO (110), *i.e.* a peak also shifts to lower 2θ values with higher T_{dep}. Due to the small amount of BZO in the YBCO matrix, the diffractograms are too noisy that the differences in the FWHMs of the curves could reliably be seen.

Cross-sectional TEM images of low-, mid- and high-T samples (Fig. 2) show significant differences in the films. In the low-T sample there are splayed nanocolumns with a width of 4.5–5.5 nm and a splaying angle of about 15°–30° with respect to the *c*-axis. In the mid-T sample there are well-aligned rods with a width of 6–7 nm. According to this image, the rods are separated by about 10–15 nm. The high-T sample has equally aligned nanocolumns with a width of 4–8 nm, but they are shorter than in the mid-T sample. Also, a large number of stacking faults parallel to the *ab*-plane are observed. The rod diameters have in all the cases been extracted from a single image and they may not always be representative samples. Therefore, it cannot be said that the rod diameters in different temperature ranges would differ significantly. According to energy dispersive X-ray spectroscopy, the rods in all the samples do not consist merely of BZO but

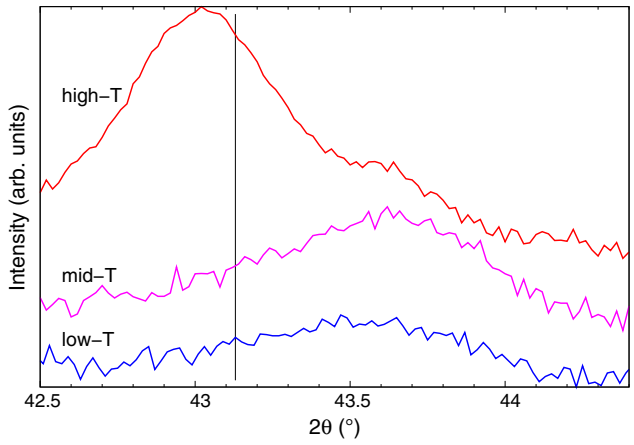

Fig. 1. The evolution of BZO (002) peak with deposition temperature. The black vertical line shows the 2θ-value of bulk BZO. The intensities have been shifted for readability.